Available online www.jsaer.com

***Journal of Scientific and Engineering Research*, 2018, 5(10):168-178**

Research Article

ISSN: 2394-2630
CODEN(USA): JSERBR

Design and Stress Analysis on a Diseased Coronary Artery Model using Finite Element Analysis

Jared May[1], Rajeev Nair[2]*

[1]AGC Automotive Americas, Elizabethtown, Kentucky, USA
[2]Department of Mechanical Engineering, Wichita State University, Wichita, Kansas, USA

Abstract Disease associated with the buildup of atherosclerotic plaque in the coronary arteries has a high mortality rate in the world. The most common of these diseases is coronary artery disease. Contemporary procedures involve placing an implant known as a stent in the offending artery. A stent acts as a scaffolding structure that holds and compresses the atherosclerotic plaque and reopens the diseased artery. A common concern with coronary stents is mechanical failure due to cyclic pressures associated with the systolic and diastolic pressures of the heartbeat. A study of the coronary artery using finite element analysis is a good way to get a first-hand glimpse of the various stresses acting on it. A quarter and full model design and numerical analysis of a simple model of the coronary diseased artery is performed and the results show interesting stress variation across the layers of the artery. These results could impact stent design and analysis for future *in-vitro* studies.

Keywords Myocardial Infarction, Hyperelastic, Artery, Stents, Finite Element Analysis, stress

1. Introduction

The artery is a passageway that transports oxygen rich blood from the myocardium to the rest of the human body. Myocardial infarction occurs when the heart muscle does not receive enough oxygen to properly function. The cells in the myocardium then begin to die due to oxygen starvation. A healthy artery consists of three layers: the intima, the media, and the adventitia. The layers of the artery are composed of two major fibers: elastin and collagen. Elastin is a non-linear elastic material. It has an incremental Young's modulus of $3*10^5$ Pa at a strain of 40% [1]. Collagen is a stiffer material possessing a Young's modulus of 10^8 Pa at a strain of 3% to 4% [1]. These two fibers act in tandem to give the artery its elastic and structural properties. The endothelium is a portion of the intima that contacts the blood. The intima consists of collagen fibers. The intima is the thinnest layer of the artery and does not serve a significant role in the artery's structural integrity. The media has different compositions throughout the human body. Larger coronary arteries consist of elastin fibers [1]. These elastin fibers give larger arteries a high degree of elasticity. Smaller arteries are made up of smooth muscle as well as a matrix of elastin and collagen. Smaller arteries are less elastic than their larger counterparts. The adventitia is exclusively made up of collagen fibers. The adventitia is the arteries main structural component of the artery. Arteries are subjected to pre-tensioning stresses in the body which serve to tether the artery to the surrounding connective heart tissue. This *in-vivo* tethering allows the artery to move in both the radial and longitudinal directions [1]. It is well documented that an artery that is removed from the body will undergo a significant reduction of length [2]. The artery length can have a reduction of up to 50% the original length. This reduction indicates an *in-vivo* arterial pre-tensioning. Therefore, an artery removed from the body is said to be in a no-load state. Fung proposed that an artery placed *in-vitro* can be returned to its *in-vivo* state by stretching the artery along its central longitudinal axis [3]. The artery is a complex mechanical structure. The artery does not have a linear stress and strain relationship. Therefore, it is difficult to determine an exact Young's modulus for

the artery. An incremental Young's modulus can be calculated using assumptions that the artery is an incompressible and isotropic material. Hasting provides means for calculating the incremental Young's modulus for an artery based upon assumptions of pseudo-elasticity [1].

$$E_{inc} = \frac{\Delta P R_o R_i^2 2(1-v^2)}{\Delta R_o (R_o^2 - R_i^2)} \quad (1.1)$$

Where: R_o is the outer artery radius, $R_i$is the inner artery radius, ΔR_o is the change in outer radius due to a pressure, ΔP is the change in pressure and v is the Poisson's Ratio. A more accurate view of the artery's elastic nature can also be modeled using deformable continuum mechanics theory. The artery does not have a linear stress/strain relationship and can therefore be can be modeled as a hyperelastic solid. A hyperelastic solid can be defined using a strain density function based upon the principles stretches of the material. The basic form of the artery's constitutive equation is shown below.

$$U^{def} = C_{ij}(I_1 - 3)^i (I_2 - 3)^j + \sum_{i=1}^{N} \frac{1}{D_1}(J_{el} - 1)^{2i} \quad (1.2)$$

Where: U^{def} is the material strain density function, C_{ij} is a material constant (the subscripts i and j describe the direction), I_1 is the first Cauchy strain invariant, I_2 is the second Cauchy strain invariant, D_1 is the material compressibility factor, J_{el} is material elastic volume strain. The Cauchy stress invariants are defined in terms of the principle stresses. The first and second Cauchy stress invariants can be defined as follows (λ is the principal stretch).

$$I_1 = \lambda_U^2 + 2\lambda_U^{-1} \quad (1.3)$$

$$I_2 = \lambda_U^{-2} + 2\lambda_U \quad (1.4)$$

There are various components of an atherosclerotic plaque. One such component of plaque is the calcified plaque. Calcified atherosclerosis is associated with an aged lesion which tends to possess an increased collagen density similar to the collagen densities found in bone [4]. Calcification typically accumulates in the intima layer of the artery. The calcification leads to intimal thickening and hardening. The arterial calcification process is almost identical to that process found in the formation of bone. Osteopontitn and osteonectin have been found in calcified intima layers [5] and are minerals found in bone formation. Atherosclerotic plaque also consists of lipids. Lipids consist of crystalline cholesterol, cholesteryl, and phospholipids [6]. The lipid core of the atherosclerotic plaque forms through the accumulation of fatty streaks that are rich with lipid cells [7]. Lipid concentration can influence the intensity of the mechanical stresses within the atherosclerotic plaque. A larger lipid core can lead to higher stresses within the plaque and artery [8]. The lipid concentration has been known to lead to a structure weakening of the arterial wall [9]. These stresses can then lead to plaque rupture and myocardial infarction. The lipid core forms between the fibrous cap and the intimal layer. A third component of atherosclerotic plaque is a fibrous cap. The fibrous cap is made up of smooth muscle tissue, extracellular material (collagen, proglycans, and elastin fibers) [6]. The fibrous cap covers the vulnerable lipid core and necrotic smooth cells [10]. Plaque rupture can occur if the fibrous cap is thin. The thin fibrous cap acts as a stress concentrator and thus can rupture under relatively low physiological forces. Significant research has gone into the study of arterial wall mechanics and intravascular stent response. Early and Kelly [11] studied the impact of arterial geometry and material properties on stents. The significance of this study was to define the mechanical properties of the intimal, medial, and adventitial layers of the artery wall and found that these layers are isotropic and incompressible. This nature can be defined by a third order Mooney-Rivlin strain energy function. The strain density function developed by Early and Kelly [11] is given below.

$$W = C_{10}(I_1 - 3) + C_{01}(I_2 - 3) + C_{20}(I_1 - 3)^2 + C_{11}(I_1 - 3)(I_2 - 3) + C_{30}(I_1 - 3)^3 \quad (1.5)$$

Where: W is the strain energy function, C is a material constant, I_1 is the first Cauchy strain invariant, and I_2 is the second strain invariant. Further studies have also been done to investigate the mechanical properties of atherosclerotic plaques. Maher et al. studied the mechanical response of atherosclerotic plaques from fresh carotid arteries [12]. This study was performed on a total of fourteen atherosclerotic plaques which consisted of calcified, lipid, and fibrous atherosclerotic plaques. The plaques were found to be isotropic, incompressible

hyperelastic materials. The data from the study was fit to a second order polynomial hyperelastic strain energy function.

$$W = C_{10}(I_1 - 3) + C_{01}(I_1 - 3) + C_{20}(I_1 - 3)^2 + C_{11}(I_1 - 3)(I_2 - 3) + C_{02}(I_2 - 3)^2 \quad (1.6)$$

Where: W is the strain energy function, C is a material constant, I_1 is the first strain invariant, and I_2 is the second strain invariant. Cervera studied the impact of stenting of the behavior of the arterial wall [13]. He modeled the artery as an idealized, hollow cylinder that was stretched by 59% of its length in order to simulate axial tethering. Matlab was used to create parametric stent geometries. The stents were parameterized in order to include the best features from other stent designs and was used to optimize stent strut spacing, axial amplitude, and the stent's curvature radius. The FEA study involved inflating the artery in order to provide luminal dilation. Each stent created through the parametric study were tested in the artery model and analyzed for critical stresses. It was found that stent geometry influences the magnitude of the stresses present in the arterial wall after stenting. The influence of pulse pressure and compression from the artery also led to an increase in stent hoop stresses [14]. Timmins et al. determined that the stent design not only affects the structure integrity of the stent but also the stress concentration in the artery. This finding indicated that there must be a compromise between stent structural integrity and arterial wall stresses [15]. The majority of these studies were performed on peripheral arteries that are subjected to bending and pulmonary arteries that are subjected to respiration.

2. Mathematical Formulation of the Artery Design and Numerical Stress Analysis

A three dimensional model of an artery and its stenotic plaque will also be created. The artery and plaque will be modeled to represent the *in-vivo* physiological state. This will involve using the FORTRAN programming language to develop an Abaqus® subroutine that will model the artery's hyperelastic behavior. The specific subroutine will be an Abaqus® Standard uhyper routine. The uhyper routine allows for Abaqus® to use complex compressible and incompressible hyperelastic material models. This uhyper routine requires that partial derivatives of the hyperelastic strain energy function be defines with respect to the strain invariants [16 – 18]. The subroutine will be tested using two dimensional arterial cross sections.The artery will be modeled in its *in-vitro* phase. Once an artery is removed from the body, it elastically recoils. This recoil indicates that a stent removed from the body is in a no load stated and an artery that is *in-vivo* is in a loaded state [3]. The no load model of the stent will be axially stretched in order to simulated the artery's *in-vivo* conditions.

2.1. Artery and Atherosclerosis Mechanics and Modeling

Early and Kelly found that the arterial layers (intima, media, and adventitia) can be modeled as an isotropic material [11]. Furthermore, Early and Kelly found that each respective layer exhibits an incompressible hyperelastic nature. Maher et al. also found that fibrous, calcified, and lipid plaques can be modeled using an incompressible hyperelastic strain energy function [12]. The general form of the polynomial hyperelastic strain energy function is shown below [16 – 18].

$$U^{def} = C_{ij}(I_1 - 3)^i (I_2 - 3)^j + \sum_{i=1}^{N} \frac{1}{D_1}(J_{el} - 1)^{2i} \quad (2.1)$$

Where: U^{def} is the strain energy function, C_{ij} is a material constant, $I_1$is the first Cauchy stress invariant, $I_2$is the second Cauchy stress invariant, D_1 is the material compressibility factor, and J_{el} is the elastic volume strain or third Cauchy invariant (λ_u is the material principle stretch). The Cauchy invariants are defined using principle material stretches.

$$I_1 = \lambda_u^2 + 2\lambda_u^{-1} \quad (2.2)$$

$$I_2 = \lambda_u^{-2} + 2\lambda_u \quad (2.3)$$

An incompressible hyperelastic material has a D_1 value that is equal to zero. This corresponds to a Poisson's ratio of 0.5. The Poisson's ratio can be defined as shown in the following equation.

$$v = \frac{3\frac{K_o}{\mu_o} - 2}{6\frac{K_o}{\mu_o} + 2} \tag{2.4}$$

Where: v is the Poisson's ratio, K_o is the bulk modulus, and μ_o is the shear modulus. The incompressibility is further defined using the third Cauchy invariant, J_{el}. The third invariant is equal to one in an incompressible hyperelastic solid. The deformation gradient thus becomes:

$$g = \sum_{i=1}^{N} \frac{1}{D_1} \left(J_{e1} - 1\right)^{2i} = \sum_{i=1}^{1} \frac{1}{0} (1-1)^2 = \infty \tag{2.5}$$

The infinite deformation gradient leads to a solid that does not change volume when undergoing strain.The incompressibility of a hyperelastic solid can also be described using the principle stretches. Lai et al. showed that an incompressible solid has an equilibrium state shown below [19].

$$x_1 = \lambda_1 x_1 \tag{2.6}$$

$$x_2 = \lambda_2 x_2 \tag{2.7}$$

$$x_3 = \lambda_2 x_3 \tag{2.8}$$

Where: x is the longitudinal direction andλ is the principle stretch in the longitudinal direction. An incompressible solid possesses an equilibrium state between the first and second principle stretches.

$$\lambda_1 \lambda_2^2 = 1 \tag{2.9}$$

This equilibrium state leads to an isochoric response in the material [19]. The isochoric response indicates no change in the material's volume during stretch. Early and Kelly defined the artery layers using a third order Mooney-Rivlinhyperelastic function [11]. The Mooney-Rivlin strain energy function is a special case of the polynomial strain energy function. The Mooney-Rivlin strain energy function is defined below.Table 1 shows the material constant values in megapascals (MPa).

$$U = C_{10}(I_1 - 3) + C_{01}(I_2 - 3) + C_{20}(I_1 - 3)^2 + C_{11}(I_1 - 3)(I_2 - 3) + C_{30}(I_1 - 3)^3 + \frac{1}{D_1}(J_{el} - 1)^2 \tag{2.10}$$

Table 1: Artery Layer Hyperelastic Constants (MPa) [11]

	C_{10}	C_{01}	C_{20}	C_{11}	C_{30}
Intima	0.08423	0.00505	1.5	0.76506	0.04238
Media	0.00355	0.00066	0.02154	0.01868	0.01977
Adventitia	0.00714	0.00063	0.00803	0.09579	0.09931

Maher et al. defined the atherosclerotic plaque using a second order polynomial strain energy function [12].Table 2 contains the material constants for three varieties of atherosclerotic plaque in MPa.

$$U = C_{10}(I_1 - 3) + C_{01}(I_2 - 3) + C_{20}(I_1 - 3)^2 + C_{11}(I_1 - 3)(I_2 - 3) + C_{30}(I_2 - 3)^2 + \frac{1}{D_1}(J_{el} - 1)^2 \tag{2.11}$$

Table 2: Atherosclerotic Plaque Hyperelastic Constants (MPa) [12]

	C_{10}	C_{01}	C_{20}	C_{11}	C_{30}
Fibrous	0.00753	0.00999	0.02063	0.00039	0.00078
Lipid	0.00116	0.01168	0.00858	0.0006	0.00022
Calcified	0.001144	0.01357	0.06238	0.02626	0.00761

A FORTRAN subroutine was written in order to implement the aforementioned strain energy functions in Abaqus®. In particular, auhyper routine was written to model the hyperelastic nature of the artery and plaque. The Abaqus® manuals recommend that incompressible materials be modeled as nearly incompressible [16-18]. A bulk modulus to shear modulus ratio of 10,000 was used to model a nearly compressible behavior. A bulk to shear modulus ratio of 10,000 leads to a Poisson ratio of 0.4995. A fully incompressible hyperelastic solid has a Poisson ratio of 0.5. Therefore, a Poisson ratio of 0.49995 has some compressibility.

$$\frac{K_o}{\mu_o} \approx 10,000 \tag{2.12}$$

$$v = \frac{3\frac{K_o}{\mu_o} - 2}{6\frac{K_o}{\mu_o} + 2} \approx 0.49995 \tag{2.13}$$

A bulk modulus to shear modulus ratio of 10,000 led to an approximate Poisson's ratio of 0.49995. Therefore, the material compressibility factor (D_1) became non zero. The compressibility factor for each arterial layer and atherosclerotic plaque were recalculated to obtain a nearly incompressible hyperelastic response. The compressibility factor is a function of the material's Poisson's ratio and the linear components of the strain energy function (C_{10} and C_{01}).Table 3 shows the D_1 values for each artery layer and plaque component.

$$D_1 = (1-2v)(C_{10} + C_{01}) \tag{2.14}$$

Table 3: Hyperelastic Compressibility Factors (MPa)

Component	***D_1 Value***
Intima	0.000008928
Media	0.000000421
Adventitia	0.00000077
Calcified	0.0000014714
Lipid	0.000001284
Fibrous	0.000001752

The uhyper subroutine also required that partial derivatives with respect to the strain invariants (I_1, I_2, and J_{el}) be calculated. The partial derivatives defined the elastic response of the strain energy function. These partial derivatives are $\frac{\delta U}{\delta I_1}$, $\frac{\delta U}{\delta I_2}$, $\frac{\delta U}{\delta J}$, $\frac{\delta^2 U}{\delta I_1^2}$, $\frac{\delta^2 U}{\delta I_2^2}$, $\frac{\delta^2 U}{\delta J^2}$, $\frac{\delta^2 U}{\delta I_1 \delta I_2}$, $\frac{\delta^2 U}{\delta I_1 \delta J}$, $\frac{\delta^2 U}{\delta I_2 \delta J}$, $\frac{\delta^3 U}{\delta I_1^2 \delta J}$, $\frac{\delta^3 U}{\delta I_2^2 \delta J}$, $\frac{\delta^3 U}{\delta I_1 \delta I_2 \delta J}$, $\frac{\delta^3 U}{\delta I_1 \delta J^2}$, $\frac{\delta^3 U}{\delta I_2 \delta J^2}$, and $\frac{\delta^3 U}{\delta J^3}$. These are the partial derivatives for the artery's Mooney-Rivlin strain energy function. The uhyper subroutine ignores any partial derivative that is equal to zero. Therefore, these partial derivatives are ignored in the following calculations.

$$\frac{\delta U}{\delta I_1} = C_{10} + C_{11}(I_2 - 3) + C_{20}(2I_1 - 6) + 3C_{30}(I_1 - 3)^2 \tag{2.15}$$

$$\frac{\delta U}{\delta I_2} = C_{01} + C_{11}(I_1 - 3) \tag{2.16}$$

$$\frac{\delta U}{\delta J} = \frac{2J - 2}{D_1} \tag{2.17}$$

$$\frac{\delta U}{\delta I_1^2} = 2C_{20} + 3C_{30}(2I_1 - 6) \tag{2.18}$$

$$\frac{\delta^2 U}{\delta J^2} = \frac{2}{D_1} \tag{2.19}$$

$$\frac{\delta^2 U}{\delta I_1 \delta I_2} = C_{11} \tag{2.20}$$

The partial derivatives for the plaque components were calculated. The plaque components were modeled using a second order polynomial hyperelastic strain energy function.

$$\frac{\delta U}{\delta I_2} = C_{10} + C_{11}\left(I_2 - 3\right) + C_{20}\left(2I_1 - 6\right) \tag{2.21}$$

$$\frac{\delta U}{\delta I_2} = C_{10} + C_{11}\left(I_1 - 3\right) + C_{30}\left(2I_2 - 6\right) \tag{2.22}$$

$$\frac{\delta U}{\delta J} = \frac{2J - 2}{D_1} \tag{2.23}$$

$$\frac{\delta^2 U}{\delta I_1^2} = 2C_{20} \tag{2.24}$$

$$\frac{\delta^2 U}{\delta I_2^2} = 2C_{30} \tag{2.25}$$

$$\frac{\delta^2 U}{\delta J^2} = \frac{2}{D_1} \tag{2.26}$$

$$\frac{\delta^2 U}{\delta I_2 \delta_2} = C_{11} \tag{2.27}$$

3. Design Modeling and Finite Element Analysis

The equations developed in the previous section were compiled into a FORTRAN subroutine. The subroutine was tested using a combination of two dimensional and three dimensional artery models. A two dimensional quarter model was first created in order to test the subroutine and boundary condition assumptions. The artery was modeled in relation to the left anterior descending artery (LAD). Suter et al. prescribed artery layer thickness to lumen diameter ratios [21]. The LAD was modeled using the mean lumen diameter of 4.38 mm. The artery was also modeled using the mean outer diameter of 5.45 mm. Holzapfel et al. investigated the ratio of artery layer thickness to artery wall thickness [22]. It was found that ratios for the adventitia, media, and intima were 0.4, 0.36, and 0.27 respectively. These ratios were used to model the artery layer thicknesses. A two dimensional quarter model of the diseased artery was created by adding a calcified intima, lipid core, and fibrous cap. Figure 1 illustrates the quarter model.

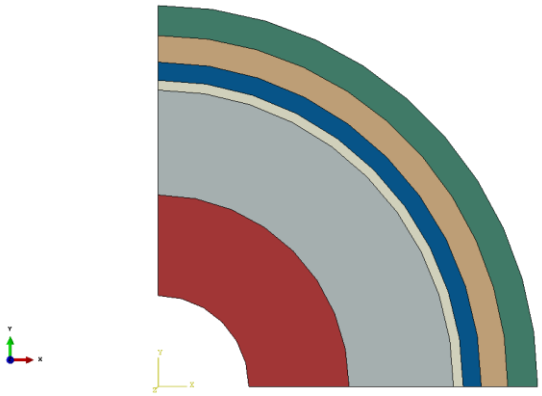

Figure 1: Artery quarter model (green is adventitia; brown is media; blue is intima; white is calcified plaque; grey is lipid core plaque; red is fibrous cap plaque)

The model was meshed using a global seed factor of 0.05. The mesh used CPS4 shell elements. A boundary condition of U_2 equals zero was applied to the nodes along the x axis. Boundary conditions of U_1 equals zero were applied to nodes along the y axis. A boundary condition on degree of freedom U_1 is synonymous with the X axis while U_2 is synonymous with the Y axis. A pressure of 0.013 MPa was applied to the lumen surface of the model. This pressure corresponded to the mean blood pressure through the artery. Figure 2 shows the mesh and boundary conditions.

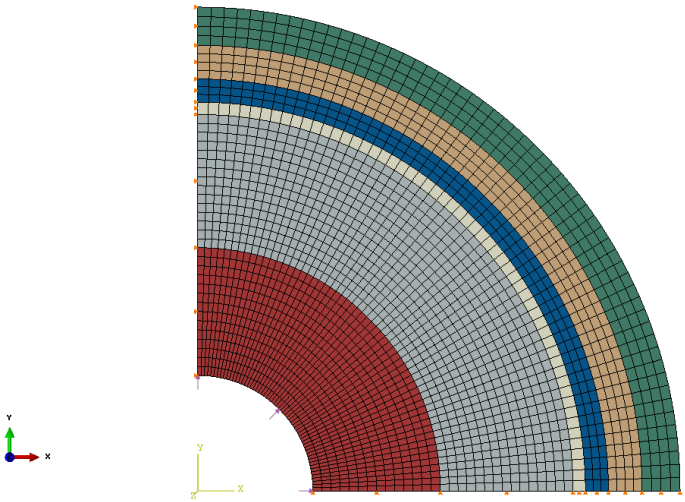

Figure 2: Quarter model mesh and boundary conditions

The quarter model was also extended to a two dimensional full model. The same meshing and boundary conditions were applied to the full model. Figure 3 shows the boundary conditions for the model.

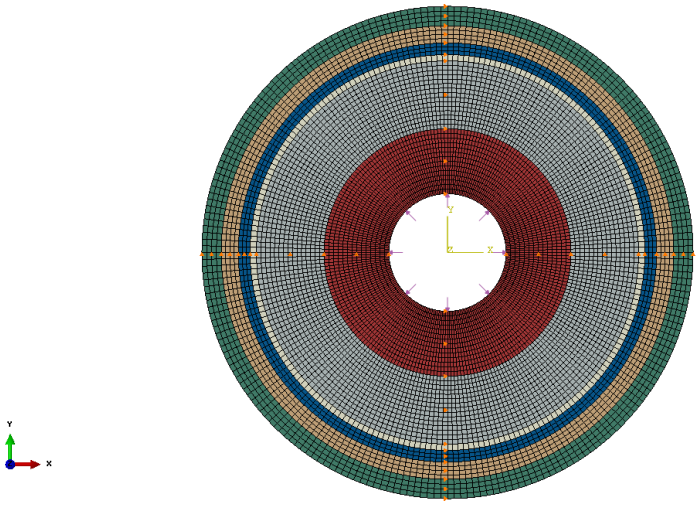

Figure 3: Full model mesh

It is well known that an *in-vivo* artery is in a loaded stated [3]. A healthy artery can be stretched up to 50% of its original *in-vitro* length. This *in-vivo* tethering allows the artery to evenly distribute the blood pressure along the endothelium. Fox et al. showed that the LAD can have a length of 32 mm [22]. Therefore, an *in-vivo* LAD is stretched by 50%; adding a 16 mm to the total length. A three dimensional model of the LAD was created using the in vitro length of 32 mm. Displacement boundary conditions of 8 mm were applied in the axial direction. These boundary conditions were applied on both the proximal and distal faces of the artery. Symmetry boundary conditions were also applied to the nodes along the x axis and y axis. Hybrid mesh elements were used to mesh the artery. Hybrid elements enforce a Poisson's ratio of 0.5 in the stiffness matrix. This helped to model the incompressible nature of the arterial wall layers. C3D8H eight node solid brick elements were used to capture the stresses induced by arterial tethering. Figure 4 shows the three dimensional model with the prescribed boundary conditions.

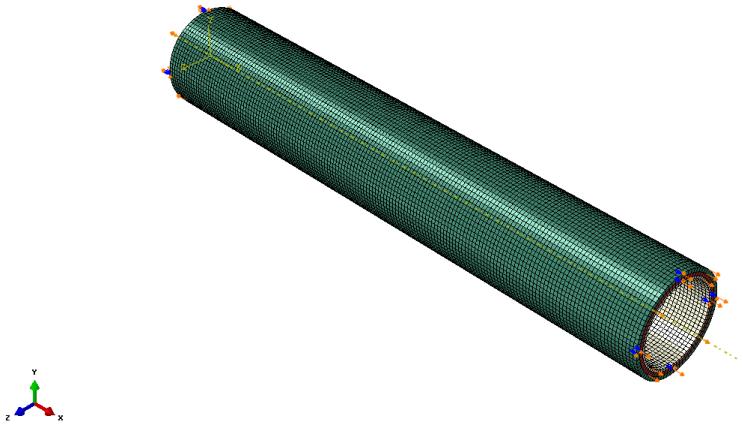

Figure 4: Arterial tethering mesh and boundary conditions

4. Results and Discussion

The stresses induced by the mean blood pressure is shown is Figure 5. This quarter model von Mises plot show an uniform circumferential distribution of stress radiating outside with the highest intensity seen in the middle as expected and gradually reducing. The middle part of the artery layer adventitia sandwiched between the other two layers seems to generate a lot more stress compared to the other layers.

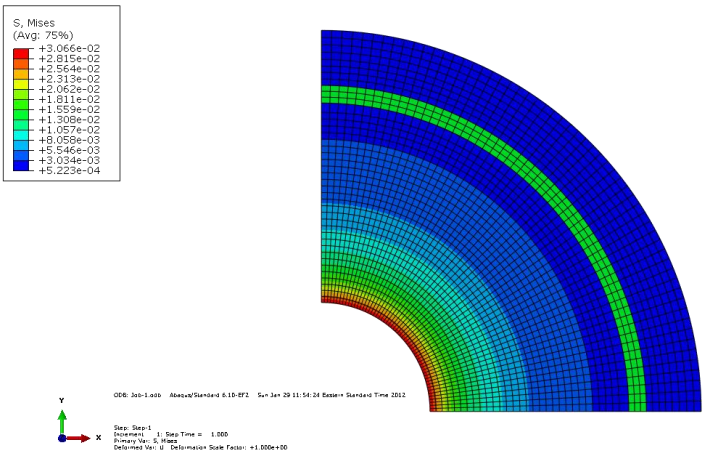

Figure 5: Quarter model von Mises stress (MPa)

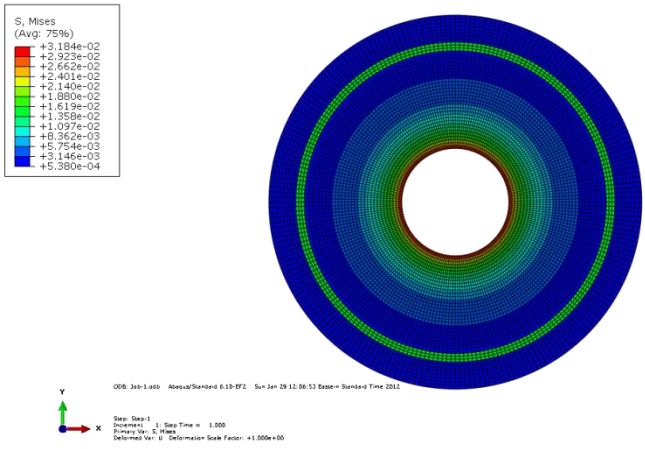

Figure 6: Full model von Mises stress (MPa)

Figure 6 shows the Von Mises stresses for a full model. The pattern seen above in figure 5 is repeated here as expected.

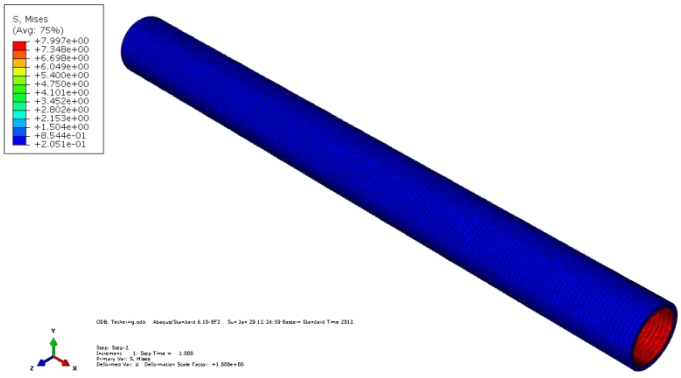

Figure 7: In-vivo arterial layer residual stresses (MPa)

Von Mises stresses (figure 7) and nodal displacement (figure 8) was monitored to determine the residual state of the *in-vivo* artery as a three-dimensional model. The *in-vivo* artery residual stresses clearly indicate the majority of the stresses pocketed deep within the inside diseased plaque layers. Clearly these inside layers are much brittle and certainly far away from a hyperelastic material property regime, and the presence of these residual stresses increases the gravity of the situation by causing problems during stent insertion, restenosis, thrombosis and myocardial infraction.

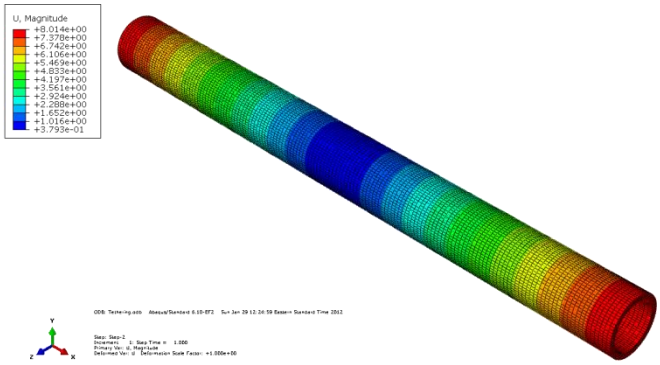

Figure 8: Tethered artery displacement

With regards to the nodal displacements, the von Mises stress was contained within the load bearing adventitia and media layers. The thin intimal layer also had stress concentration. The nodes on the front and back faces of the artery were displaced using a displacement boundary condition in the X direction. The nodes on the front face were displaced 8 mm and the nodes on the back face were displaced negative 8 mm. A mean pressure of 0.013 MPa was applied to the tethered artery model. The boundary and mesh conditions from the tethering model were obtained in order to model the *in-vivo* state. Figure 13 illustrates the blood pressure induced stresses.

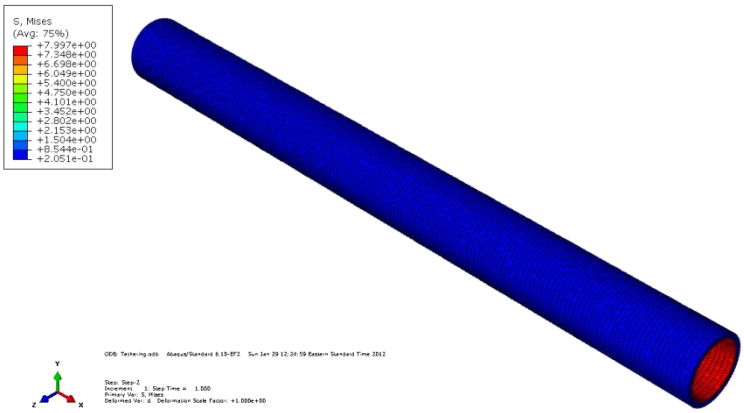

Figure 9: Arterial stresses due to blood pressure (MPa)

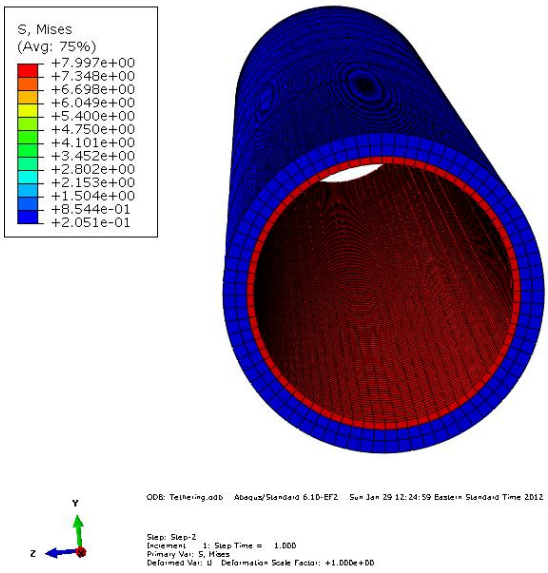

Figure 10: Stresses along the arterial lumen due to blood pressure

The blood pressure induced a localized stress within the intimal layer. As it is known, the intima serves to isolate the blood from the media and adventitia. The artery model showed the axial load bearing nature of the adventitia and media. It also indicated the blood pressure regulating nature of the intima.

5. Conclusions

Diseased coronary artery with the three layers of arterial tissue (intima, media and adventitia) and the three layers of plaque (lipid core, fibrous core, calcified plaque) was modeled by using Mooney-Rivlin equations and various subroutines like 'uhyper' using the finite element software Abaqus. These equations were used to get material properties of hyperlelastic material like the artery with important material constants and other relevant information from the literature that has used *in-vitro* studies to come up with the most accurate results. Quarter model, full 2D model and a full 3D model of the diseased artery was constructed with good approximation and meshed with a reasonably accurate mesh size and boundary conditions based on an *in-vivo* mode. Some of the interesting conclusions from the study are as follows. The quarter model shows the value of von Mises stresses to be in reasonably good agreement with literature displaying a maximum of 0.03 MPa in the inside intima layer and average of 0.013 MPa throughout the model. It can also be seen that the stress variation shows a gradual decline towards the outside in a radiating pattern. The only exception is the inside adventitia layer that shows an increased stress concentration compared to its surrounding layers. It is hypothesized that the material property of adventitia and its interaction with the other two arterial layers causes this phenomenon. The full2D model shows the value of von Mises stresses to be in reasonably good agreement with literature displaying a maximum of 0.032 MPa in the inside intima layer and average of 0.013 MPa throughout the model. It can also be seen that the stress variation shows a gradual decline towards the outside in a radiating pattern. The only exception is the inside adventitia layer (like for the quarter model) that shows an increased stress concentration compared to its surrounding layers. It is hypothesized that the material property of adventitia and its interaction with the other two arterial layers causes this phenomenon. The full 2D model is a little more accurate than the quarter model. For the 3D model, the *in-vitro* displacement and residual stresses show a similar pattern as the quarter and the 2D model, but with a better accuracy as expected. Since a displacement condition was applied here based on realistic scenarios as explained in the literature, arterial stresses along the lumen around 8 MPa was achieved. This study has shown a realistic view on a diseased artery and the stresses and displacements that are commonly seen.

References

[1]. Hastings, G. W. (1992). *Cardiovascular Biomaterials.* London: Springer-Verlag.

[2]. Green, S. I., Schajer, G. S., Parker, D. R., & Post, A. J. (1995, November). *In vivo* Measurement of Arterial Pre-Tension. *Medical and Biological Engineering and Computing*.
[3]. Fung, Y. C. (Ed.). (2002). *Introduction to Bioengineering* (Vol. 2). River Edge, New Jersey: World Scientific.
[4]. Fitzpatrick, L. A., Edwards, W. D., & Ingram, R. T. (1994). Diffuse Calcification in Human Coronary Arteries. *The Journal of Clinical Investiation, 94*, 1597-1604.
[5]. Bobryshev, Y. V., Lord, R., & Warren, B. A. (1995). Calcified Deposit Formation in Intimal Thickenings of the Human Aorta. *Atherosclerosis, 118*, 9-21.
[6]. Sirol, M. (2006). Atherosclerosis Plaque Imaging and Characterization Using Magnetic Resonance Imaging. *US Cardiology*, 1-5.
[7]. Ross, R. (1993, April 29). The Pathogenesis of Atherosclerosis: A Perspective for the 1990s. *Nature, 362*, 801-809.
[8]. Huang, H., Virmani, R., Younis, H., Burke, A. P., Kamm, R. D., & Lee, R. T. (2001). The Impact of Calcification on the Biomechanical Stability of Atherosclerotic Plaques. *Circulation, 103*, 1051-1056.
[9]. Guyton, J. R., & Klemp, K. F. (1989). The Lipid-Rich Core Region of Human Atherosclerosis Fibrous Plaques: Prevalence of Small Lipid Droplets and Vesicles by Electron Microscopy. *The American Journal of Pathology, 134*(3), 705-717.
[10]. Bennett, M. R. (2007). The Atherosclerotic Plaque Was Not Built in a Day: The Dynamic Nature of Plaque Progression and Instability. *Heart and Metabolism, 36*, 5-7.
[11]. Early, M., & Kelly, D. J. (2010). The Role of Vessel Geometry and Material Properties on the Mechanics of Stenting in the Coronary and Peripheral Arteries. *224*(3).
[12]. Maher, E., Creane, A., Sultan, S., Hynes, N., & Lally, C. (2009). Tensile and Compressive Properties of Fresh Human Carotid Atherosclerotic Plaques. *Journal of Biomechanics, 7*(32).
[13]. Cervera, J. (2006). *Stent Design and Arterial Mechanics: Parameterization Tools Using the Finite Element Method*. Texas A&M University, Biomedical Engineering. College Station: Texas A&M University.
[14]. Li, N., & Gu, Y. (2005). Parametric Design Analysis and Shpe Optimization of Coronary Artery Stent Structure. *World Congresses of Structural and Multidisciplinary Optimization.* Rio de Janeiro,Brazil.
[15]. Timmins, L. H., Moreno, M. R., Meyer, C. A., Criscione, J. C., Rachev, A., & Moore, J. E. (2007). Stented Artery Biomechanics and Device Design Optimization. *Medical and Biological Engineering and Computing, 45*, 505-513.
[16]. Simulia. (n.d.). Abaqus Analysis User's Manual.
[17]. Simulia. (n.d.). Abaqus Theory Manual.
[18]. Simulia Centrail. (2011). *Adjustable Rigid Torus (ART)*. (Simulia) Retrieved January 2, 2012, from Extensions for Abaqus: http://www.simulia.com/products/rsurf.html
[19]. Lai, W. M., Rubin, D., & Krempl, E. (2010). *Introduction to Continuum Mechanics* (4 ed.). Oxford: Elsevier.
[20]. Suter, Y., Schoenenberger, W., Toggweiler, S., Jamshidi, P., Resink, T., & Erne, P. (2009). Intravascular Ultrasound-Based Left Main Coronary Artery Assessment: Comparision Between Pullback from Left Anterior Descending and Circumflex Arteries. *21*(9).
[21]. Holzapfel, G. A., Sommer, G., Gasser, C. T., & Regitnig, P. (2005). Determination of Layer-Specific Mechanical Properties of Human Coronary Arteries with Nonatherosclerotic Intimal Thickening and Related Constitutive Modeling. *American Journal of Physiology: Heart and Circulatory Physiology, 289*, 2048-2058.
[22]. Fox, C., Davies, M. J., & Webb-Peploe, M. M. (1973). Length of Left Main Coronary Artery. *35*.